ACS APPLIED MATERIALS & INTERFACES

Examining MRI Contrast in Three-Dimensional Cell Culture Phantoms with DNA-Templated Nanoparticle Chains

Hamsa Jaganathan,[†] Daniel L. Hugar,[†] and Albena Ivanisevic[*,†,‡]

[†]Weldon School of Biomedical Engineering, Purdue University, West Lafayette, Indiana 47906, United States

[‡]Department of Chemistry, Purdue University, West Lafayette, Indiana 47906, United States

Supporting Information

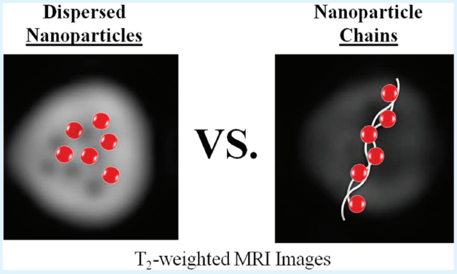

ABSTRACT: DNA-templated nanoparticle (NP) chains were examined as potential magnetic resonance imaging (MRI) contrast agents using in vitro environments of the extracellular matrix and tissue. A 3-T clinical MRI scanner was utilized to examine and compare image contrast enhanced by dispersed NPs, DNA-templated NP chains, gold-superparamagnetic multicomponent NP chains, and polyelectrolyte encapsulated, multicomponent NP chains in both T_1-weighted and T_2-weighted images. In addition, the longitudinal and transverse relaxivity (r_1 and r_2) changes were measured both in the basement membrane, using Matrigel, and in the tissue environment, using in vitro 3D cell culture scaffolds. Results suggest that MRI contrast was significantly enhanced from NP chains compared to dispersed NPs in the basement membrane and polyelectrolyte encapsulation for NP chains produced similar relaxivity to nonencapsulated NP chains due to the enhanced cell uptake of encapsulated NP chains.

KEYWORDS: MRI, nanoparticle chains, matrigel, gold, superparamagnetic, in vitro

INTRODUCTION

Magnetic resonance imaging (MRI) agents improve image contrast by selectively relaxing surrounding protons in tissues to enhance MRI signals. Contrast agents aid to clearly visualize distinct locations of injured or tumor sites. The safety of the agent and the effectiveness to produce distinct image contrast between normal and abnormal tissues are two factors to consider when developing MRI contrast agents for in vivo systems.[1] Currently used contrast agents that have been approved by the U.S.Food and Drug Administration (FDA) are composed of the paramagnetic element, gadolinium.[2] These MRI contrast agents, however, produce low magnetic fields because of their proton relaxation mechanism and have been exhibited to induce kidney toxicity.[3] Therefore, there is a need to develop effective contrast agents that are safer than gadolinium-based agents. In recent years, superparamagnetic nanoparticles (NPs) have shown a great promise to serve as contrast agents for MRI applications.[4]

Superparamagnetic NPs have exhibited to be less toxic and have greater magnetization (10- to 1000-fold) than paramagnetic materials. Compared to gadolinium chelates, the single-crystal arrangement of superparamagnetic NPs produces a greater magnetization and therefore, stronger local magnetic fields to enhance surrounding proton relaxation.[5−8] Superparamagnetic NPs influence protons through transverse relaxation because of the accelerated dephasing of proton spins from the local inhomogenous magnetic fields, producing negative contrast in T_2-weighted MRI images.[1] Although they demonstrate great promise as a new generation contrast agent, their design properties, such as surface type, size, and structure, affect their function under in vivo conditions. Therefore, majority of research efforts are focused on modifying the (1) surface, (2) size, or (3) structure of superparamagnetic NPs.

Positively charged surfaces on NPs bind to cells nonspecifically, whereas, negatively charged surfaces of NPs rapidly internalize by the liver.[9,10] In general, however, studies have demonstrated that a neutral surface increases blood circulation times.[11] In addition, surface coatings, such as dextran, poly(ethylene glycol), albumin, silica, and others have demonstrated to be a biocompatible covering to stabilize the NPs. With regards to size, NPs that are intravenously administered are in the size order of 5−150 nm to avoid rapid renal clearance.[12]

The rate of nanostructure uptake in organs, blood circulation time, renal clearance are all important factors to consider when designing a nanostructures for in vivo MRI applications. A typical, clinical MRI exhibits low sensitivity in the orders of 1×10^{-3} to 1×10^{-5} mol/L and a temporal resolution in the orders of minutes to hours.[13] To acquire a strong MRI signal, contrast agents are required to exhibit long blood circulation times (hours) to provide the scanner more time for quality signal detection.[14] Iron oxide NPs (5 nm) have demonstrated to have short blood circulation times (in the order of seconds to minutes.[1] Besides increasing the diameter of the NPs, another approach to increase blood circulation time is to manipulate the structure. Linear, one-dimensional (1D) structures, such as carbon nanotubes[14−18] and filaments,[19] have exhibited prolonged half-blood lives and blood clearance compared to spherical-shaped nanostructures. Recently, a number of researchers

Received: January 22, 2011
Accepted: March 7, 2011
Published: March 07, 2011

ACS Publications © 2011 American Chemical Society

Scheme 1. Schematic of the Different Types of Nanostructures (nanoparticles, single-component NP chains, multicomponent NP chains, and layer-by-layer encapsulated multicomponent NP chains) Used to Examine and Compare MRI Contrast Enhancement in 3D Cell Culture Systems

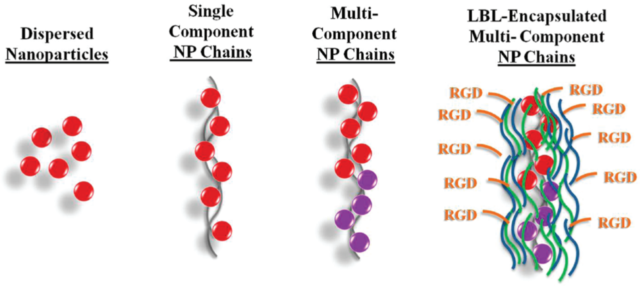

have been developing and characterizing 1D iron oxide NP chains,[20−36] which may aid to enhance their utility as MRI contrast agents.

Our lab has examined the proton relaxation properties for DNA-templated NP chains. It was found that arranging NPs along DNA produced greater relaxivity than dispersed NPs in NMR experiments.[37,38] A higher relaxivity represents the sensitivity of the contrast agent. In other words, the relaxivity value measures how well surrounding protons are able to relax in the presence of low concentrations of the contrast agent. In addition, we have examined the changes in relaxation properties for multicomponent NP chains, or the joining of gold NP chains to iron oxide NPs chains.[39] It was observed that there were segmental interactions among the multicomponent chains causing differences in proton relaxation times in NMR. These experiments provided information regarding the material's characteristics on proton relaxation. These past studies, however, lacked the biologically and clinically relevant information on the potential MRI application for DNA-templated NP chains.

In this study, the contrast differences in the presence of DNA-templated NP chains for the extracellular matrix and 3D cell culture scaffolds are examined in a 3 T clinical MRI scanner. The 3T MRI scanner would provide clinically relevant data on the potential effectiveness of DNA-templated NP chains as MRI contrast agents. The use of basement membrane and 3D cell culture scaffolds as phantoms aid to understand proton relaxation effects in a biological environment. Using in vitro tools, such as 3D cell culture scaffolds, to study the effects under a biological environment is an intermediate step between preliminary material characterization in NMR and in vivo experiments regarding information on pharmacokinetics and toxicity in animals.[40] Although the in vivo properties can influence the performance of a drug, it is important to obtain preliminary information on the effectiveness of the drug under in vitro conditions. Herein, MRI contrast for the in vitro environment is examined and compared (1) between dispersed NPs and NP chains to understand the influence of structure, (2) between multicomponent NP chains and mixed solution of dispersed magnetic and metallic NPs to understand the influence of composition, and (3) between nonencapsulated and polyelectrolyte-encapsulated NP chains to understand the influence of surface coating (Scheme 1). The in vitro MRI results collected are compared to results found in NMR experiments to identify the changes in proton relaxation in a biological environment and would provide preliminary information on the potential performance of the contrast agent before in vivo testing.

■ EXPERIMENTAL METHODS

Materials. Gold NP conjugates (5 nm) with poly-L-lysine were purchased from Ted Pella, Inc. (Redding, CA). Iron oxide and cobalt iron oxide NPs (5 nm) coated with pyrrolidinone were synthesized and characterized in our lab, following the procedure in Li et al.[41] Unmethylated lambda-DNA, MULTI-CORE buffer, *Eco*RI, T4 DNA ligase were purchased from Promega. Poly(styrene sulfonate) (PSS, MW ∼70 000) and poly(allylamine hydrochloride) (PAH, MW ∼70 000) were purchased from Sigma-Aldrich. The peptide, KKKKKKRGD (MW 1116.4, purity >95%), was synthesized and purified by Biosynthesis Inc. (Lewisville, TX).

Fabrication of Single- and Multicomponent DNA-Templated NP Chains. Prior to the fabrication of NP chains, gold NPs were washed in water by centrifuging 10 min at 13 000 rpm. The washing process was repeated three to five times. The NP washing process was necessary due to the evidence of unwashed gold NPs inducing cellular toxicity.[42] NP chains were fabricated by the self-assembly of positively charged nanoparticles with naturally negatively charged DNA. An equal mass of nanoparticles (gold, iron oxide, or cobalt iron oxide) were added an equal mass of DNA in a buffered solution and vortexed for 1 h at room temperature, creating single component NP chains.[43,44] An example image of DNA-templated nanostructures is provided in Figure S1 in the Supporting Information. Characterization of formation has been published in the literature.[45] Multicomponent NP chains were fabricated using DNA specific enzymes. *Eco*RI (1 unit/1 μg DNA) was added to the solution of single component NP chains. The restriction enzyme reaction was performed at room temperature for 4 h and the reaction was terminated at 65 °C for 30 min. To create 0.1:1:0.9 Au:DNA:Fe_2O_3 mass ratio for gold−iron oxide multicomponent NP chains, 87% volume of restriction enzyme cut iron oxide NP chains were mixed with 13% volume of restriction enzyme cut gold NP chains and T4 DNA ligase (1 unit/1 μg DNA) was added to the mixed solution. The ligation reaction was performed at room temperature for 30 min and terminated at 65 °C for 15 min, forming multicomponent NP chains.[46−50] Gold−cobalt iron oxide multicomponent NP chains were fabricated similarly using restriction enzyme cut cobalt iron oxide NP chains. Single- and multicomponent NP chains were filtered before diluting in cell medium.

Fabrication of Layer-by-Layer Encapsulation. Filtered multicomponent NP chains were encapsulated using the layer-by-layer method in a washless process.[51] Washless process was chosen due to the difficulty in washing DNA-NP constructs.[52−55] The fabrication and characterization of layer-by-layer encapsulation can be found in previously published literature.[37,38,42] In short, PSS and PAH (1 mg/mL) are alternatively layered on multicomponent NP chains. As the eighth layer, RGD peptides were layered as the cell targeting molecule for integrin surface receptors on HT-29 cells. Samples were then diluted in cell medium. The stability of these nanostructures in serum-filled cell medium was measured previously.[42]

Culturing HT-29 Cell Line. HT-29 cell line, human colon cancer cells, were purchased from American Type Culture Collection and cultured with McCoy's 5A medium (ATCC). Cells were maintained in 37 °C in an atmosphere of 5% CO2 and 95% relative humidity in T-25 cell culture flasks. Fresh medium supplemented with 10% fetal bovine serum (ATCC) was changed twice a week and passed every week, as cells were 50% confluent in 2 days.

Preparation of 3D Cell Cultures using Matrigel. Matrigel was purchased from BD Biosciences. Nanostructure−Matrigel phantoms for MRI scanning were made by mixing nanostructures with Matrigel and cell medium and pipetted into 96 well plates at four different

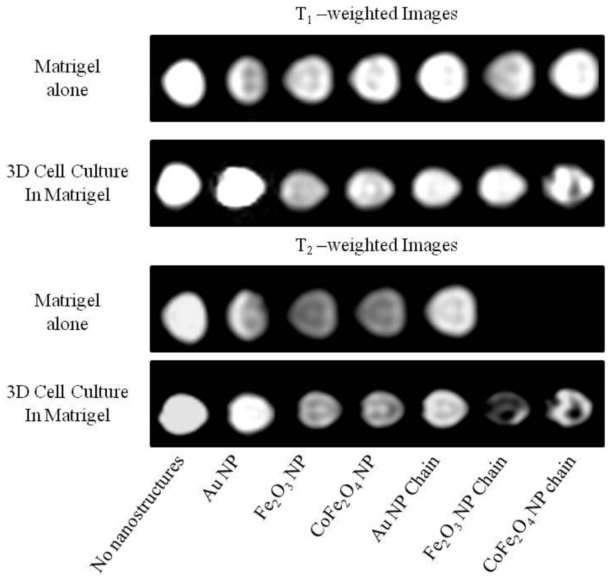

Figure 1. T_1-weighted and T_2-weighted magnetic resonance images comparing contrast between dispersed NPs and NP chains for gold, iron oxide, cobalt iron oxide in Matrigel, and 3D cell scaffolds.

Table 1. Transverse Relaxivity Measured for Single-Component and Multicomponent NP chains in Matrigel and in 3D Cell Culture Compared to Dispersed Nanoparticles (highlighted values represent significant difference in relaxivity ($n = 3$, $p = 0.05$) and value represents mean ± standard deviation)

		r_2 (mM^{-1} s^{-1})	
	nanostructure materials	dispersed NPs	NP chains on DNA
in Matrigel	single component		
	Au	10.1 ± 5.8	10.0 ± 6.0
	Fe_2O_3	12.2 ± 0.3	78.6 ± 35.0
	$CoFe_2O_4$	21.7 ± 15.6	114.0 ± 34.0
	multicomponent		
	$Au-Fe_2O_3$	9.7 ± 6.0	120.4 ± 12.6
	$Au-CoFe_2O_4$	21.3 ± 1.5	89.5 ± 11.0
cells in Matrigel	single component		
	Au	5.0 ± 1.2	2.5 ± 2.0
	Fe_2O_3	4.6 ± 3.4	12.3 ± 8.0
	$CoFe_2O_4$	8.0 ± 4.7	11.8 ± 7.4
	multicomponent		
	$Au-Fe_2O_3$	7.2 ± 4.0	8.8 ± 3.2
	$Au-CoFe_2O_4$	6.0 ± 4.0	13.3 ± 6.4

nanoparticle concentrations. After the nanostructure/Matrigel mixture was incubated for 30 min in 37 °C, the Matrigel phantoms were ready to be scanned in MRI. Alternatively, 3D cell cultures were prepared following the protocol from Lee et al.[56] Confluent cells were washed with sterilized PBS and detached from the flask using 0.25% Trypsin/EDTA (ATCC). After spinning down in a centrifuge (125 g, 7 min), cells were resuspended in fresh medium. To form the 3D embedded cell cultures, cells mixed with Matrigel are added into a Matrigel coated 96-well plate. The well plate was then incubated at 37 °C for 30 min and fresh medium was then added to the wells. The 3D cell culture is maintained for a week, changing the medium every two days. After 1 week, nanostructures were diluted in serum-filled medium and treated to the three-dimensional cell cultures for 2 days. Four different concentrations of nanostructures were treated to the cells. After 2 days of treatment and prior to the MRI experiments, excess medium from the wells was removed and washed three times with sterilized PBS. Samples were incubated in sterilized PBS before MRI scanning.

MRI Experiments. Matrigel and 3D cell culture phantoms in 96-well plates were scanned using a clinical 3 T Whole Body GE HDx Imager (General Electric Healthcare, Waukesha, WI). A transmit/receive knee coil array was used for data acquisition. To acquire T_1-weighted images, the inversion recovery (IR) pulse sequence was used with following parameters: inversion time (TI) = 4000 ms, repetition time (TR) = 6000 ms, FOV = 12 cm, slice thickness =1.6 mm, 0 mm spacing, echo train length =2, and acquisition matrix =128 × 128. For T_1 time measurements, eight scans were acquired with different inversion times (TI = 100−4000 ms) to collect a series of data. To acquire T_2-weighted images, fast spin echo (FSE-XL) pulse sequence was used set at the following parameters: echo time (TE) = 301.0 ms, repetition time (TR) = 6000 ms, FOV = 12 cm, slice thickness = 1.6 mm, 0 mm spacing, echo train length =32, and acquisition matrix =128 × 128. For T_2 time measurements, eight scans with different echo times (TE = 9.4−301.0 ms) to collect a series of data points. The T_1 and T_2 relaxation time was calculated by fitting on a pixel-by-pixel basis using the two curves: $M(TI) = M_0^*(1-2\exp(-TI/T_1))$ and $M(TE) = M_0^*\exp(-TE/T_2)$, respectively. This calculation was performed in Matlab R10.0 (MathWorks, Massachusetts).

After calculating the longitudinal ($R_1 = 1/T_1$) and transverse relaxation ($R_2 = 1/T_2$), longitudinal and transverse relaxivity, r_1 and r_2, were measured by fitting the data in a linear relationship between relaxation and NP concentration. Linear regression analysis to calculate the longitudinal and transverse relaxivity was performed in STATA 10.0 (StataCorp LP, College Station, TX). Significance tests among relaxivity averages were performed using one-way analysis of variance in STATA 10.0 (StataCorp LP, College Station, TX). MRI scans was performed on three separate Matrigel and 3D cell culture samples at the 95% confidence interval.

RESULTS AND DISCUSSION

MRI Contrast between NPs and NP Chains. In order to understand the influence of NP structure on proton relaxation and therefore contrast enhancement, MRI scans were collected for Matrigel and 3D cell culture phantoms, comparing between dispersed NPs and NP chains for gold, iron oxide, and cobalt iron oxide compositions (Figure 1). In T_1-weighted images, no significant changes in image contrast were observed between gels without nanostructures and gels with NPs and NP chains. Gold is a diamagnetic material and therefore, has a weak magnetic interaction to influence the relaxation of surrounding protons. The lack of proton relaxation enhancement in the presence of gold material for both NPs and NP chains corresponds to no difference in image contrast in T_1-weighted and T_2-weighted MRI images. Superparamagnetic NPs and NP chains influence the transverse proton relaxation times (T_2) more than the longitudinal proton relaxation times (T_1), and therefore, did not produce contrast differences in T_1-weighted MRI images.

Table 1 lists the transverse (r_2) relaxivity measured from the MRI scans. The longitudinal (r_1) relaxivity rates measured are found in Table S1 in the Supporting Information. Relaxivity is used to quantify the efficacy of MR contrast agents, in which the value represents how well the relaxation rate increases with contrast agent concentration. There was no significant difference in the r_1 averages between NPs and NP chains in both Matrigel and the 3D cell culture phantoms. In addition, the ratio, r_2/r_1, were high values greater than 1, indicating these nanostructures exhibit low sensitivity as T_1-contrast agents and have a greater utility as T_2-contrast agents.

In T_2-weighted images, however, changes in proton relaxation and therefore, image contrast is observed between NPs and NP chains. When iron oxide and cobalt iron oxide NP chains were mixed in Matrigel phantom, T_2-weighted images exhibited a darker contrast compared to the Matrigel phantom mixed with dispersed iron oxide and cobalt iron oxide NPs. In quantitative terms, there was a significant difference in transverse relaxivity averages between superparamagnetic NP chains ($r_2^{\text{iron oxide}} = 78.6 \pm 35.0\ \text{mM}^{-1}\ \text{s}^{-1}$) and dispersed NPs ($r_2^{\text{iron oxide}} = 12.2 \pm 0.3\ \text{mM}^{-1}\ \text{s}^{-1}$). A high relaxivity produced a dark contrasted image of the Matrigel phantom in T_2-weighted MRI images.

Initially, NMR was used to measure changes in the proton relaxation because the presence of the nanostructures in water.[37] The high sensitivity in NMR aided understanding of the mechanism of proton relaxation. When superparamagnetic NPs are arranged along the DNA strand, the clustering and assembly of the NPs produced a collective magnetic behavior, increasing the magnetization of the NP chain. The increased magnetization directly corresponds to an increase in the local magnetic field strength, influencing surrounding protons to transversely relax faster compared to the local magnetic fields produced by dispersed NPs. This observation was similarly found in nanoworms, a one-dimensional (1D) structure with 5−10 nm iron oxide NP.[33] The enhanced spin−spin relaxation of water protons was caused by the increased magnetization and NP assembly. In the Matrigel phantom, this same proton relaxation behavior was observed.

Longitudinal and transverse relaxation times depend on water molecule dynamics and the physical and chemical environment, and therefore, it is expected that the times measured in NMR experiments performed in deuterated water would be different from the times measured in Matrigel phantom MRI experiments.[57] Matrigel resembles the basement memebrane and is made up of extracellular matrix materials. It is a meshwork of collagen, elastin, fibronectin, laminin, and proteoglycans and is commonly used for drug toxicology, angiogenesis, and tumor invasion studies.[40] The basement membrane is mostly responsible for the survival and differentiation of the epithelium cellular layer. Therefore, the use of the Matrigel as a phantom in these MRI studies aids to improve our understanding on the efficiency of these nanostructures as MRI contrast agents in a tissue environment. By mimicking the tissue environment, the function and efficiency of MRI contrast agents can be assessed inexpensively prior to examining in animal models.

The addition of cells in Matrigel produces 3D cell culture scaffolds. When cancer cells are grown in Matrigel, multicellular 3D spheroids with characteristic 3D cell to cell junctions are formed, resembling tumor tissue with regards to its cell shape.[58] The 3D cancer cell spheroids exhibit typical histological characteristics of a tumor. By mimicking the in vivo tissue architecture of cancer tumors, the efficiency of nanostructures as cancer detection agents can be evaluated in a more realistic environment than testing in 2D cell culture systems. In 2D culture systems, cells lack the structural architecture and transport properties that are observed in vivo.[59] Most cancer drug studies are performed and tested in 3D cell culture scaffolds prior to using an animal model. The microenvironment found in 3D cell culture scaffolds is essential as it replicates cell to cell and cell to matrix interactions.[60] These interactions affect regulatory mechanisms for cell growth and differentiation, as well as the penentration and action of drugs, such as MRI contrast agents.[61,62] In this study, colon cancer cells were cultured in Matrigel to mimic the architecture of colon cancer tumors.[63]

In our previous study, we observed in transmission electron microscope (TEM) images that both positively charged NPs and NP chains were nonspecifically internalized in 2D colon cancer cell culture (example shown in Figure S2 in the Supporting Information).[42] There was no significant difference in the amount of nanostructure uptake for both dispersed NPs and NP chains. The cell uptake was not governed by the nanostructure shape. Since NP chains are flexible structures, they were clustered similarly to NPs alone and internalized by vesicles in the cytoplasm of the cells. When observing the MRI contrast in T_2-weighted images for 3D cell culture phantoms treated with superparamagnetic nanostructures, there was no significant difference in relaxivity averages between NPs ($r_2^{\text{iron oxide}} = 4.6 \pm 3.4\ \text{mM}^{-1}\ \text{s}^{-1}$) and NP chains ($r_2^{\text{iron oxide}} = 12.3 \pm 8.0\ \text{mM}^{-1}\ \text{s}^{-1}$). This finding indicates that the efficiency for in vitro cell uptake governs the MRI contrast signal for these nanostructures. The clustering of nanostructures in the cell's cytoplasm produced similar proton relaxation behavior for both NPs and NP chains. In general, the transverse relaxivity measured in the tumor-mimicking 3D cell culture phantoms were lower than the transverse relaxivity measure in the extracellular matrix Matrigel phantoms. The difference in proton relaxation is attributed to the differences in the microstructure of the tissues.[57] When working with in vivo models, however, cell uptake is not the only parameter that determines the efficiency of contrast agents. Parameters such as blood circulation, immune system activation, biodistribution, and tumor targeting efficiency are issues that need to be addressed and evaluated.

MRI Contrast Using Multicomponent NP Chains. In addition to understanding the structural influence (NPs vs NP chains) on proton relaxation, the composition influence on proton relaxation is also of interest. In a publication from Zabow et al.,[64] it was found that microstructures composed of a metallic spacer sandwiched in between magnetic disks enhanced proton behavior. The size of the magnetic disks, the length of the metallic spacer, and the overall structure produced various proton frequency shifts. This type of design is relevant for studies in multispectral MRI, in which different cell types would be tagged with different nanostructure designs, producing corresponding proton relaxation signals to a specific cell type. In efforts to emulate this idea in NP chains, multicomponent NP chains made with gold and magnetic (iron oxide or cobalt iron oxide) NPs were easily fabricated using DNA-specific enzymes.

The two types of DNA-specific enzymes used to fabricate multicomponent DNA-templated NP chains are restriction enzymes and DNA ligase. Type II Restriction enzymes recognize specific base sequences on double-stranded DNA and are able to cleave the DNA strand at the sequence. We previously demonstrated that *Eco*RI, a type II restriction enzyme, is able to cut NP-coated DNA strands.[46,48] Multicomponent DNA templated NP chains are fabricated with DNA segments coated with gold NPs are joined together with DNA segments coated with iron oxide NPs. The joining, or the gluing, of DNA strands is achieved through T4 DNA ligase. This enzyme is able to recognize enzyme-cleaved DNA strands and joins them by making phosphodiester bonds. This technique of cutting and gluing DNA strands with enzymes is commonly used in genetic recombinant engineering and is adaptable to form gold−iron oxide and gold−cobalt iron oxide NP chains.

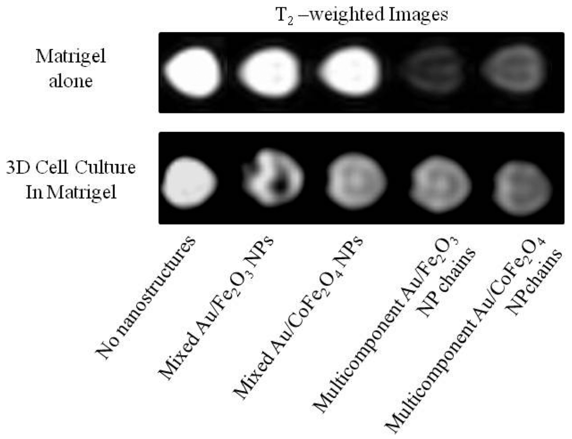

Figure 2. T_2-weighted magnetic resonance images comparing contrast between mixed gold and magnetic dispersed NPs and gold-magnetic NP chains in Matrigel and 3D cell culture phantoms.

Previous NMR experiments indicated that the transverse proton relaxation times for gold—iron oxide and gold—cobalt iron oxide NP chains can be controlled by the amount of magnetic NP chains available in solution.[39] It was found that the joining of the gold segments to superparamagnetic segments created intersegmental interactions. These interactions influenced the proton relaxation differently from the relaxation observed with single-component NP chains. The MRI results listed in Table 1 are comparable to the NMR findings. The transverse relaxivity for single component NP chains ($r_2^{\text{iron oxide}}$ = 78.6 ± 35.0 $\text{mM}^{-1}\ \text{s}^{-1}$) were different than the transverse relaxivity for multicomponent NP chains ($r_2^{\text{Au}-\text{Fe}_2\text{O}_3}$ = 120.4 ± 12.6 $\text{mM}^{-1}\ \text{s}^{-1}$) in Matrigel phantoms. The difference between the relaxivity averages, however, was not statistically significant. The discrepancy in the finding between NMR and MRI may be caused by the addition of extracellular proteins and growth factors in the Matrigel phantom. The nonspecific binding of proteins to the nanostructures may have caused clustering and agglomeration for both single- and multi- component NP chains, producing statistically similar transverse proton relaxivity.

In T_1-weighted MRI images (see Figure S3 in the Supporting Information), no change in image contrast for Matrigel and 3D cell culture phantoms was observed among the control (no nanostructures), mixed solution of gold and magnetic NPs, and multicomponent gold-magnetic NP chains. In T_2-weighted images (Figure 2); however, MRI contrast was observed between multicomponent NP chains ($r_2^{\text{Au}-\text{Fe}_2\text{O}_3}$ = 9.7 ± 6.0 $\text{mM}^{-1}\ \text{s}^{-1}$) and mixed solution of gold and magnetic NPs ($r_2^{\text{Au}+\text{Fe}_2\text{O}_3}$ = 120.4 ± 12.6 $\text{mM}^{-1}\ \text{s}^{-1}$) in Matrigel phantoms (Table 1). The arrangement of NPs on DNA strands, as well as possible nonspecific agglomeration with extracellular proteins, may have produced greater proton relaxivity for multicomponent NP chains than for mixed, dispersed metallic and magnetic NP solution. This finding was consistent with results observed in another type of multicomponent contrast agent containing iron oxide NPs around gold nanorods.[36] The metallic component of the nanostructure did not hinder the proton relaxation because of the linear arrangement of the superparamagnetic NPs.

In the T_2-weighted MRI images of 3D cell culture phantoms, no significant difference in contrast was observed between mixed NPs and multicomponent NP chains. As discussed earlier, TEM images indicated that cells internalized and agglomerated NPs and NP chains similarly into vesicles located in the cytoplasm.[42] The agglomeration of nanostructures in the vesicles produced comparable proton relaxations for NPs and NP chains.

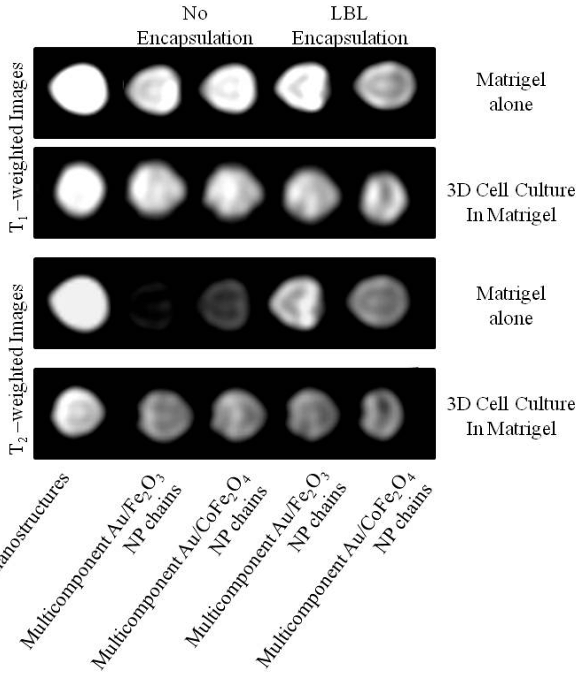

Figure 3. T_1-weighted and T_2-weighted magnetic resonance images comparing contrast between unencapsulated and LBL-encapsulated multicomponent NP chains in Matrigel and 3D cell culture phantoms.

MRI Contrast after Layer-by-Layer Encapsulation. To improve specific cell uptake of nanostructures, surface encapsulation is a simple solution. Recently, we studied the proton relaxivity changes due to surface encapsulation in NMR.[38] Using the layer-by-layer method, negatively- and positively- charged polyelectrolytes are alternatively layered on the surface of NP chains. At the outermost layer, RGD-terminated poly-L-lysine peptides were coated on the surface. RGD peptides are specific ligands to human colon cancer cells as it binds to the integrin cell surface receptors. The addition of targeting ligands on the surface of the MRI contrast agent would aid to improve in cell uptake. NMR results indicated that surface encapsulation of the NP chains decreased transverse relaxivity compared to nonencapsulated NP chains. Surrounding water protons did not experience strong local magnetic fields from the encapsulated NP chains because of the surface coverage of the polyelectrolytes. The proton relaxation mechanism was discussed extensively and nonencapsulated and LBL-encapsulated NP chains were observed to validate the outer-sphere theory for proton relaxation.

A similar proton relaxation trend was observed in T_2-weighted MRI images of Matrigel phantoms (Figure 3). Table 2 displays that the transverse relaxivity for LBL-encapsulated, multicomponent NP chains ($r_2^{\text{Au}-\text{Fe}_2\text{O}_3}$ = 75.4 ± 8.1 $\text{mM}^{-1}\ \text{s}^{-1}$) was lower than nonencapsulated, multicomponent NP chains ($r_2^{\text{Au}-\text{Fe}_2\text{O}_3}$ = 120.4 ± 12.6 $\text{mM}^{-1}\ \text{s}^{-1}$). Conversely, the longitudinal relaxivity for both encapsulated and nonencapsulated NP chains were low (see Table S2 in the Supporting Information) and displayed no significant image contrast in T_1-weighted MRI images.

Although encapsulated NP chains produced lower transverse relaxivity than nonencapsulated NP chains in water and in Matrigel phantoms, the transverse relaxivity in 3D cell culture

Table 2. Transverse Relaxivity for Unencapsulated and LBL-eEncapsulated NP Chains in Matrigel and 3D Cell Culture Phantoms

		r_2 (mM^{-1} s^{-1})	
	multicomponent DNA-templated NP chains	no encapsulation	LBL encapsulation
in Matrigel	Au−Fe_2O_3	120.4 ± 12.6	75.4 ± 8.1
	Au−$CoFe_2O_4$	89.5 ± 11.0	55.5 ± 16.6
cells in Matrigel	Au−Fe_2O_3	8.8 ± 3.2	11.8 ± 4.8
	Au−$CoFe_2O_4$	13.3 ± 6.4	6.8 ± 1.3

phantoms was not statistically different between nonencapsulated and encapsulated NP chains. For 3D cell culture phantoms, MRI contrast is governed by the in vitro cell uptake of nanostructures. It was observed that cell uptake for NP chains significantly improved after encapsulating with polyelectrolytes and targeting ligands, compared to unencapsulated NP chains. Cells were able to internalize encapsulated NP chains 3−4 times better than nonencapsulated NP chains.[42] It was found from Zhang et al. that cell internalization was a function of targeting ligand load on the nanostructure surface, rather than a function of the nanostructure's shape.[65]

In the cell, surrounding protons experience strong local magnetic fields from nonencapsulated NP chains, causing protons to relax with a transverse relaxivity of $r_2 = 8.8 \pm 3.2$ mM^{-1} s^{-1}. Although the surrounding protons near encapsulated NP chains experienced weaker local magnetic fields, the increased number of the encapsulated NP chains compared to nonencapsulated NP chains in the cells produced greater number of local magnetic fields, causing protons to relax ($r_2 = 11.8 \pm 4.8$ mM^{-1} s^{-1}) statistically equal to the proton relaxation produced from nonencapsulated NP chains. Therefore, the findings suggest that LBL encapsulation with targeting ligands on NP chains is necessary for greater cell uptake and would produce observable image contrast in T_2-weighted MRI images.

CONCLUSIONS

In conclusion, DNA-templated NP chains were examined as potential MRI agents under in vitro conditions. This study examined MRI contrast using biologically relevant environments, resembling the basement membrane and cancer tumors. Despite the presence of extracellular proteins and growth factors, the proton relaxation behavior in the basement membrane was similar to the behavior measured using NMR. It was found that cell uptake was a major factor to produce T_2-weighted image contrast enhancement in cell culture phantoms. As this study was an intermediate step between material characterization and in vivo animal studies, the results collected are relevant to understand the utility of DNA-templated NP chains as in vivo MRI agents.

ASSOCIATED CONTENT

Supporting Information. TEM and AFM characterization, additional longitudinal relaxation rates (r_1), and T_1-weighted MR images for multicomponent nanostructures (PDF). This material is available free of charge via the Internet at http://pubs.acs.org.

AUTHOR INFORMATION

Corresponding Author

*E-mail: albena@purdue.edu.

ACKNOWLEDGMENT

This work was supported by NSF under CMMI-0727927. We thank Dr. Thomas Talavage and Dr. Gregory Tamer for their assistance on MRI training and data analysis at the Purdue University MRI Facility in Innervision West Advanced Medical Imaging.

REFERENCES

(1) Na, H. B.; Song, I. C.; Hyeon, T. *Adv. Mater.* **2009**, *21*, 1–16.

(2) Caravan, P.; Ellison, J. J.; McMurry, T. J.; Lauffer, R. B. *Chem. Rev.* **1999**, *99*, 2293–2352.

(3) Sadowski, E. A.; Bennett, L. K.; Chan, M. R.; Wentland, A. L.; Garrett, A. L.; Garrett, R. W.; Djamali, A. *Radiology* **2007**, *243*, 148–157.

(4) Laurent, S.; Forge, D.; Port, M.; Roch, A.; Robic, C.; Elst, L. V.; Muller, R. N. *Chem. Rev.* **2008**, *108*, 2064–2110.

(5) Gun'ko, Y. K.; Brougham, D. F.; . In *Magnetic Nanomaterials*; Kumar, C. S. S. R., Ed.; Wiley-VCH: Weinheim, Germany, 2009; Vol. 4, pp 119−186.

(6) Burtea, C.; Laurent, S.; Elst, L. V.; Muller, R. N.; . In *Molecular Imaging I*; Semmler, W., Schwaiger, M., Eds.; Handbook of Experimental Pharmacology; Springer Verlag: Berlin, 2008; Vol. 185/1, 135−165.

(7) Duguet, E.; Vasseur, S.; Mornet, S.; Devoisselle, J.-M. *Nanomedicine* **2006**, *1*, 157–168.

(8) Geraldes, C. F. G. C.; Laurent, S. *Contrast Media Mol. Imaging* **2009**, *4*, 1–23.

(9) Ito, A.; Shinkai, M.; Honda, H.; Kobayashi, T. *J. Biosci. Bioeng.* **2005**, *100*, 1–11.

(10) Lewinski, N.; Colvin, V.; Drezek, R. *Small* **2008**, *4*, 26–49.

(11) Sun, C.; Lee, J. S. H.; Zhang, M. *Adv. Drug Deliveryv.* **2008**, *60*, 1252–1265.

(12) Neuberger, T.; Schopf, B.; Hofmann, H.; Hofmann, M.; Rechenberg, B. v. *J. Magn. Magn. Mater.* **2005**, *293*, 483–496.

(13) Massoud, T. F.; Gambhir, S. S. *Genes Dev.* **2003**, *17*, 545–580.

(14) Faraj, A. A.; Cieslar, K.; Lacroix, G.; Gaillard, S.; Canet-Soulas, E.; Cremillieux, Y. *Nano Lett.* **2009**, *9*, 1023–1027.

(15) Lacerda, L.; Herrero, M. A.; Venner, K.; Bianco, A.; Prato, M.; Kostarelos, K. *Small* **2008**, *4*, 1130–1132.

(16) Liu, Z.; Cai, W.; He, L.; Nakayama, N.; Chen, K.; Sun, X.; Chen, X.; Dai, H. *Nature Nanotechnol.* **2007**, *2*, 47–52.

(17) Liu, Z.; Davis, C.; Cai, W.; He, L.; Chen, X.; Dai, H. *Proc. Natl. Acad. Sci. U.S.A* **2008**, *105*, 1410–1415.

(18) Singh, R.; Pantarotto, D.; Lacerda, L.; Pastorin, G.; Klumpp, C.; Prato, M.; Bianco, A.; Kostarelos, K. *Proc. Natl. Acad. Sci. U.S.A* **2006**, *103*, 3357–3362.

(19) Geng, Y.; Dalhaimer, P.; Cai, S.; Tsai, R.; Tewari, M.; Minko, T.; Discher, D. E. *Nat. Nanotechnol.* **2007**, *2*, 249–255.

(20) Fakhrullin, R. F.; Bikmullin, A. G.; Nurgaliev, D. K. *ACS Appl. Mater. Interfaces* **2009**, *1*, 1847–1851.

(21) Jia, J.; Yu, J. C.; Wang, Y.-X. J.; Chan, K. M. *ACS Appl. Mater. Interfaces* **2010**, *2*, 2579–2584.

(22) Lee, C.-M.; Jeong, H.-J.; Lim, S. T.; Sohn, M.-H.; Kim, D. W. *ACS Appl. Mater. Interfaces* **2010**, *2*, 756–759.

(23) Byrne, S. J.; Corr, S. A.; Gun'ko, Y. K.; Kelly, J. M.; Brougham, D. F.; Ghosh, S. *Chem. Commun* **2004**, 2560–2561.

(24) Choi, J. H.; Nguyen, F. T.; Barone, P. W.; Heller, D. A.; Moll, A. E.; Patel, D.; Boppart, S. A.; Strano, M. S. *Nano Lett.* **2007**, *7*, 861–867.

(25) Corr, S. A.; Byrne, S. J.; Tekoriute, R.; Meledandri, C. J.; Brougham, D. F.; Lynch, M.; Kerskens, C.; O'Dwyer, L.; Gun'ko, Y. K. *J. Am. Chem. Soc.* **2008**, *130*, 4214–4215.

(26) Corr, S. A.; Gunâ€ko, Y. K.; Tekoriute, R.; Meledandri, C. J.; Brougham, D. F. *J. Phys. Chem. C* **2008**, *112*, 13324–13327.

(27) Correa-Duarte, M. A.; Grzelczak, M.; Salgueirino-Maceira, V.; Giersig, M.; Liz-Marzan, L. M.; Farle, M.; Sierazdki, K.; Diaz, R. *J. Phys. Chem. B* **2005**, *109*, 19060–19063.

(28) Fresnais, J.; Berret, J. F.; Frka-Petesic, B.; Sandre, O.; Perzynski, R. *Adv. Mater.* **2008**, *20*, 3877–3881.

(29) Jung, J. S.; Lim, J. H.; Malkinski, L.; Vovk, A.; Choi, K. H.; Oh, S. L.; Kim, Y. R.; Jun, J. H. *J. Magn. Magn. Mater.* **2007**, *310*, 2361–2363.

(30) Liu, Y.; Jiang, W.; Li, S.; Li, F. *Appl. Surf. Sci.* **2009**, *255*, 7999–8002.

(31) Nakata, K.; Hu, Y.; Uzun, O.; Bakr, O.; Stellacci, F. *Adv. Mater.* **2008**, *20*, 4294–4299.

(32) Park, J.-H.; Maltzahn, G. v.; Zhang, L.; Derfus, A. M.; Simberg, D.; Harris, T. J.; Ruoslahti, E.; Bhatia, S. N.; Sailor, M. J. *Small* **2009**, *5*, 694–700.

(33) Park, J.-H.; Maltzahn, G. v.; Zhang, L.; Schwartz, M. P.; Ruoslahti, E.; Bhatia, S. N.; Sailor, M. J. *Adv. Mater.* **2008**, *20*, 1630–1635.

(34) Salgueirino-Maceira, V.; Correa-Duarte, M. A.; Hucht, A.; Farle, M. *J. Magn. Magn. Mater.* **2006**, *303*, 163–166.

(35) Sheparovych, R.; Sahoo, Y.; Motornov, M.; Wang, S.; Luo, H.; Prasad, P. N.; Sokolov, I.; Minko, S. *Chem. Mater.* **2006**, *18*, 591–593.

(36) Wang, C.; Chen, J.; Talavage, T.; Irudayaraj, J. *Angew. Chem.,Int. Ed* **2009**, *48*, 2759–2763.

(37) Jaganathan, H.; Gieseck, R. L.; Ivanisevic, A. *Nanotechnology* **2010**, *21*, 245103.

(38) Jaganathan, H.; Gieseck, R. L.; Ivanisevic, A. *J. Phys. Chem. C* **2010**, *114*, 22508–22513.

(39) Jaganathan, H.; Gieseck, R. L.; Hudson, K.; Kellogg, M.; Ramaswamy, A. K.; Raver, K. E.; Smith, T.; Vacchiano, A. N.; Wager, A.; Ivanisevic, A. *ChemPhysChem* **2010**, *11*, 3664–3672.

(40) Reed, J.; Walczak, W. J.; Petzold, O. N.; Gimzewski, J. K. *Langmuir* **2008**, *25*, 36–39.

(41) Li, Z.; Chen, H.; Bao, H.; Gao, M. *Chem. Mater.* **2004**, *16*, 1391–1393.

(42) Jaganathan, H.; Ivanisevic, A. *ACS Appl. Mater. and Interfaces* **2010**, *2*, 1407–1413.

(43) Kinsella, J. M.; Ivanisevic, A. *Langmuir* **2007**, *23*, 3886–3890.

(44) Nyamjav, D.; Ivanisevic, A. *Biomaterials* **2005**, *26*, 2749–2757.

(45) Jaganathan, H.; Kinsella, J. M.; Ivanisevic, A. *ChemPhysChem* **2008**, *9*, 2203–2206.

(46) Jaganathan, H.; Ivanisevic, A. *Colloid Surf.*, **2008**, *67*, 279–283.

(47) Jaganathan, H.; Ivanisevic, A. *Appl. Phys. Lett.* **2008**, *93*, 263104–3.

(48) Kinsella, J. M.; Ivanisevic, A. *J. Am. Chem. Soc.* **2005**, *127*, 3276–3277.

(49) Kinsella, J. M.; Ivanisevic, A. *Colloid Surf.*, **2008**, *63*, 296–300.

(50) Kinsella, J. M.; Shalaev, M. V.; Ivanisevic, A. *Chem. Mater.* **2007**, *19*, 3586–3588.

(51) Bantchev, G.; Lu, Z.; Lvov, Y. *J. Nanosci. Nanotechnol.* **2009**, *9*, 396–403.

(52) Caruso, F.; Caruso, R. A.; Mohwald, H. *Science* **1998**, *282*, 1111–1114.

(53) Sukhorukov, G. B.; Donath, E.; Davis, S.; Lichtenfeld, H.; Caruso, F.; Popov, V. I.; Möhwald, H. *Polym. Adv. Technol.* **1998**, *9*, 759–767.

(54) Sukhorukov, G. B.; Donath, E.; Lichtenfeld, H.; Knippel, E.; Knippel, M.; Budde, A.; Möhwald, H. *Colloid Surf.*, **1998**, *137*, 253–266.

(55) Trubetskoy, V.; Wong, S.; Subbotin, V.; Budker, V.; Loomis, A.; Hagstrom, J.; Wolff, J. *Gene Ther.* **2003**, *10*, 261–271.

(56) Lee, G. Y.; Kenny, P. A.; Lee, E. H.; Bissell, M. J. *Nat. Methods* **2007**, *4*, 359–365.

(57) Stanisz, G. J.; Odrobina, E. E.; Pun, J.; Escaravage, M.; Graham, S. J.; Bronskill, M. J.; Henkelman, R. M. *Magn. Reson. Med.* **2005**, *54*, 507–512.

(58) Fischbach, C.; Chen, R.; Matsumoto, T.; Schmelzle, T.; Brugge, J. S.; Polverini, P. J.; Mooney, D. J. *Nat. Methods* **2007**, *4*, 855–860.

(59) Kim, J.; Stein, R.; O'Hare, M. *Breast Cancer Res.Treat.* **2004**, *85*, 281–291.

(60) Adissu, H. A.; Asem, E. K.; Lelievre, S. A. *Reprod. Sci.* **2007**, *14*, 11–19.

(61) Bennett, K. M.; Zhou, H.; Sumner, J. P.; Dodd, S. J.; Bouraoud, N.; Doi, K.; Star, R. A.; Koretsky, A. P. *Magn. Reson. Med.* **2008**, *60*, 564–574.

(62) Tan, M.; Wu, X.; Jeong, E.-K.; Chen, Q.; Parker, D. L.; Lu, Z.-R. *Mol. Pharm.* **2010**, *7*, 936–943.

(63) Hu, M.; Xia, M.; Chen, X.; Lin, Z.; Xu, Y.; Ma, Y.; Su, L. *Dig. Dis. Sci.* **2009**, *55*, 2365–2372.

(64) Zabow, G.; Dodd, S.; Moreland, J.; Koretsky, A. *Nature* **2008**, *453*, 1058–1064.

(65) Zhang, K.; Fang, H.; Chen, Z.; Taylor, J.-S. A.; Wooley, K. L. *Bioconjugate Chem.* **2008**, *19*, 1880–1887.